LAWRENCE
LIVERMORE
NATIONAL
LABORATORY

LLNL-TR-810542

PAL Experimental Report Form

L. E. Dresselhaus-Cooper

May 20, 2020

Disclaimer

This work performed under the auspices of the U.S. Department of Energy by Lawrence Livermore National Laboratory under Contract DE-AC52-07NA27344.

Experiment Report Form

◈ Contact Information

Principal Investigator	Leora Dresselhaus-Cooper
Affiliation	Lawrence Livermore National Laboratory

◈ Experiment Information

Proposal Number	2019-1st-NCI-037
Beamline	NCI – CXI
Experiment Run Dates	05/16/19 – 05/21/19 (mm/dd/yy – mm/dd/yy)
Proposal Title	An Ultrafast View of X-ray Induced Defect Dynamics in Cosmic Diamonds
Experiment Summary	We constructed the first simultaneous dark- and bright-field X-ray microscope in this experiment, coupling it to simultaneous measurements of the wide-angle X-ray diffraction, and the XFEL pulse intensity and energy spectrum on each shot. This experiment established proof of concept for this new advanced measurement technique and demonstrated DFXM at an XFEL for the first time. Within this complex experiment, we also acquired data that advanced our research goals within materials science and mathematics. These included: - A preliminary study of how local effects reduce the X-ray damage threshold in diamond. - A preliminary study of how X-ray radiation imparts heat into materials based on irreversible phase transitions that occur in boric acid with increasing temperature (based on hydration). - A study of X-ray radiation damage from ultrafast thermal cycling and nonthermal melting in bismuth selenide. - We also began developing software to automate alignment of compound refractive lenses (CRLs) using stochastic Nelder-Mead optimization methods. This work will expedite and improve the accuracy of alignments for many future experiments using CRLs.

Publication Report	We have manuscripts in preparation for (1) the development of the instrumentation at NCI, (2) the local effects we began to observe from X-ray radiation in diamond, (3) the evolution of structure in bismuth selenide upon rapid thermal cycling and nonthermal melting, and (4) the development of new methods to automate CRL alignment. All of these manuscripts currently require additional data to unambiguously demonstrate the high-impact results that they currently suggest. We have additional beamtime allocated at the PAL-XFEL for Directors Beamtime to complete this work, and, once travel restrictions from Covid-19 are removed, we look forward to completing this initial work. A full description of our results in each of these projects and our plans for the follow-up experiment, are included in the **Full-Page Report Form** on next page.

◈ Full Page Report Form

Please describe details of your experiments and results. You can add graphs and figures. You can explain the current status and your future plans on this experiment.

Across materials science—from dislocation junctions strengthening materials to interstitial defects fracturing batteries over many charge cycles—defects change how materials respond to their surroundings [1,2]. Defect engineers create and position point defects to finely tune a material's properties, but defects extending across many unit cells (mesoscale) can tune other material behaviors [3,4]. Existing experimental techniques have characterized the properties and dynamics of point defects [5], but those same tools have lagged for mesoscale defects [6]. As a result, a plethora of scientific questions remain unsolved that require carefully mapped mesoscale defects—especially under dynamic loading. In X-ray science, a general tool to spatially-resolve the evolution of plasticity *in-situ* and, specifically, the interactions between adjacent strain or defects, requires sub-nanosecond imaging with nm-resolution (*7*, *8*). Holography and X-ray coherent diffractive imaging (XCDI) have demonstrated this type of spatiotemporal resolution at XFEL sources [9–11], but the necessary apertures and foci at the sample prevent these methods from capturing sufficiently large field-of-view to capture statistical populations of nanoscale features [12]. While Bragg-XCDI has been able to spatially resolve the strain fields in nanoparticles [13], the same lattice-resolution measurements have not been extended to full-field X-ray imaging. High-resolution XFEL imaging in real-space (non-XCDI) has only measured the transmitted beam, making it insensitive to the sparse defects that initiate plastic transformations. To statistically probe how plasticity instigates large-scale material transformations, we need a technique with high spatiotemporal resolution and a large field-of-view that is sensitive to *both* density variation and localized strain fields inside the crystals.

Our initial work in this experiment extended DFXM to XFELs for the first time, setting up the infrastructure for it at NCI and collecting the first-ever DFXM data collected outside the ESRF. By placing a compound refractive lens (CRL) along a selected diffraction peak, DFXM collects a real-space image of a selected strain population, allowing it to resolve the individual defects buried deep within bulk, mm-sized crystals [6,14–16]. While ESRF's 0.1-s temporal resolution was limited by the integration time required to acquire each image, the high intensity available at the PAL-XFEL enabled DFXM to measure single-shot images with the 32-fs integration time of a single XFEL pulse—13 orders of magnitude faster than previously attainable. The novel framework developed at NCI used simultaneous bright-field X-ray microscopy (BFXM) to resolve the material's density variation along the transmitted beam, while collecting DFXM to resolve the local lattice distortions that caused these density changes. These two techniques gave us a snapshot of how defects (and their associated strain fields and damage) grow, propagate, interact and cascade into large-scale material transformations. Coupling these microscopes to wide-angle X-ray diffraction and measurements of the pulse energy and spectrum on each pulse, we were able to enhance our interpretation, however, we will still require additional datasets to unambiguously demonstrate our conclusions. In this experiment, we constructed the microscopes (Fig. 1) and collected the initial datasets that demonstrate some of the new phenomena that will be possible to measure with our novel technique. We will return to the PAL-XFEL for during the 2nd half of 2020 to complete these initial experiments.

Our team established proof of concept for these novel simultaneous imaging techniques during 2019-1st-NCI-037. That experiment successfully constructed ultrafast DFXM, BFXM, WAXS, in-line spectroscopy, and photon flux for each XFEL pulse. With this novel technique, we began to develop an automated CRL alignment algorithm to develop NCI's infrastructure for DFXM and collected data to study X-ray damage in three different materials—diamond, Bi_2Se_3, and H_3BO_3. We have begun drafts of 3 manuscripts from this work, but each component requires more experimental results to provide the unambiguous results necessary for the high-impact publications.

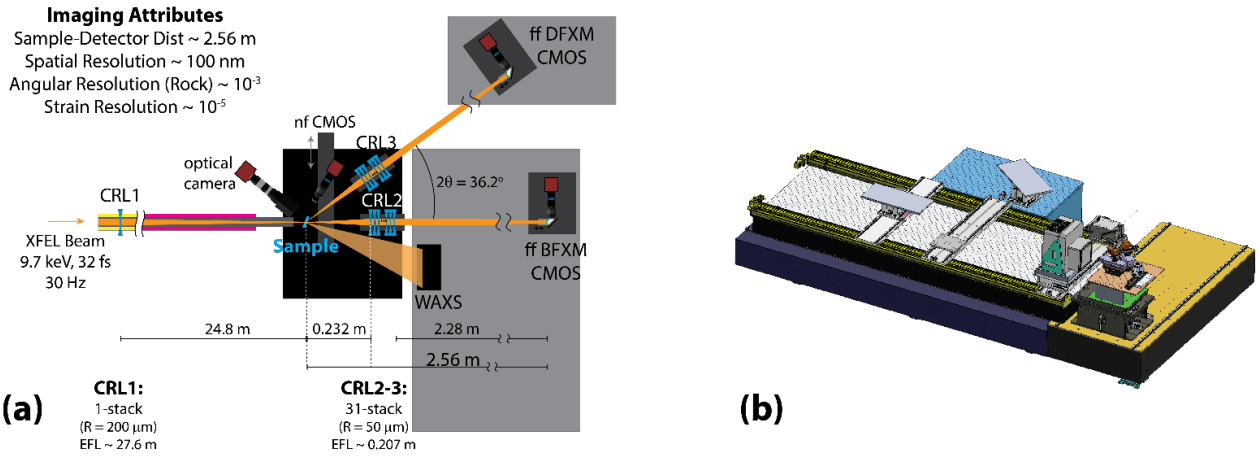

Figure 1. Proposed (and previously used) experimental design (a) and 3D model (b) for simultaneous ultrafast BFXM, DFXM, XRD and optical microscopy in the NCI hutch.

AUTOMATION: We have begun to develop custom algorithms to automate many of the complex alignments and calibrations required for our experiment. In our experiment, S Breckling established a Nelder-Mead approach (similar to gradient-descent) to align our imaging CRLs by optimizing the motor positions, reducing the alignment measurements required from ~400 to ~5 per CRL stack. For the code to run reliably at XFELs, we learned that the code needed to be adapted to make it robust to fluctuations and drift in the XFEL pulse intensity and pointing—work that has been continued since our experiment, and has been tested and refined at the Advanced Photon Source. We have also ordered a custom 2θ-stage that will simplify CRL alignment and enable strain-resolved scans. Together, the stage and automation methods will enable us to align the DFXM setup much faster and with higher precision than in our original experiments in May 2019 Our refined methodology and setup will enable future experiments to use more experimental time to measure the samples, as well as perform more detailed measurements.

DAMAGE REGIMES IN Bi_2Se_3: Previous work has found the thermoelectric material Bi_2Se_3 to be a highly sensitive material to X-ray radiation, likely caused by rapid absorption-induced thermalization (~98% absorption @ 9.7 keV). Our measurements investigated this, with WAXS measurements indicated that the initially single-crystalline material became a mosaic structure first XFEL pulse, and each subsequent XFEL pulse showing further orientational changes that were typical of crystal grain rotation. The corresponding BFXM images showed a hole forming with

complicated structures along its boundaries as the crystal orientations were shifting. Combining the results from diffraction and imaging with SEM images of the recovered sample, we clearly observed three different structures produced by the damage: sputter, disorganized nano-grains, and prismatic micro-grains. The three different types of structures suggest different damage mechanisms, likely caused by the XFEL impulsively melting the material to temperatures that dictate the types of structures that form upon cooling. By measuring the BFXM integrated intensity (normalized by the pulse energy) on each XFEL shot, we observed different slopes in the onset of damage, suggesting different mechanisms based on the XFEL flux and sample thickness. As the damage occurred in <100 shots for almost all fluxes, the complex multi-stage kinetics we observe in the lowest energy XFEL damage cannot be resolved without further measurements at even lower XFEL flux. To fully resolve the different active damage pathways, this work will repeat the initial experiments at lower XFEL fluences, to reveal the radiation load required to access each successive damage pathway. This will provide the final data required for us to publish the first simultaneous BFXM and WAXS experiments at XFELs.

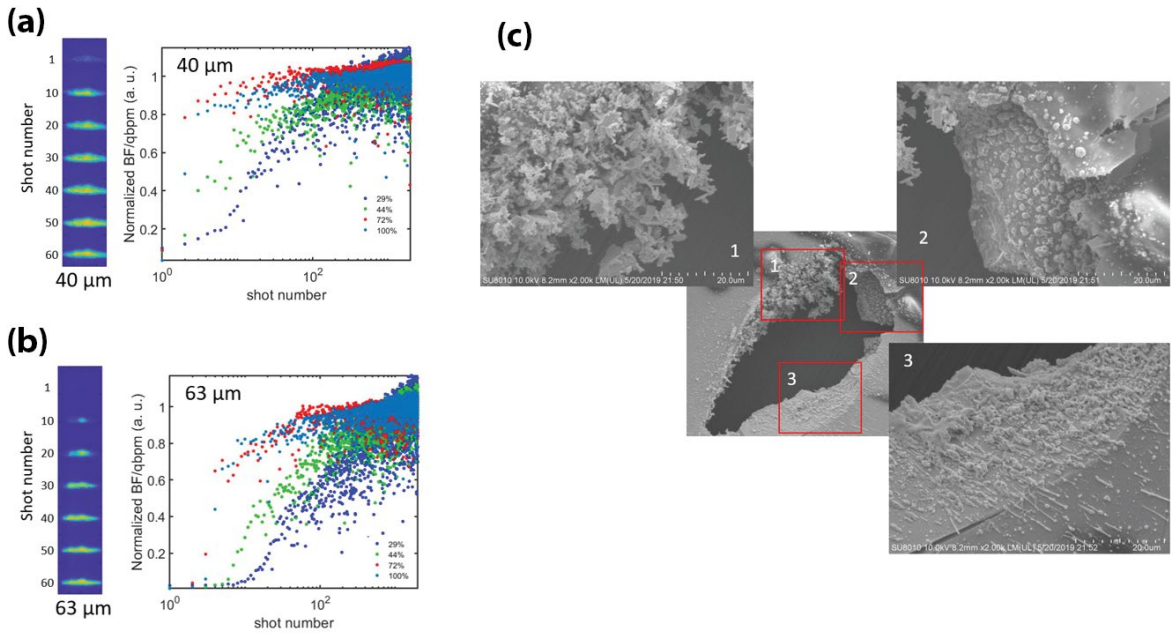

Figure 2. Data showing the onset of radiation damage in Bi_2Se_3. Selected images of the 63-µm and 40-µm thickness are shown (29% fluence) to illustrate the progression of damage based on sample thickness. Plots (a) and (b) indicate the normalized BFXM intensity on each XFEL shot, with the slope of the curves indicating different active damage pathways. These results indicate that low-flux measurements are needed to resolve the complex pathways involved in the radiation damage with this time-resolution. (c) SEM images demonstrate three different mechanisms of damage we observed, including sputter (3), recrystallization into small prismatic crystals (1), and flash recrystallization into disorganized crystalline flakes (2).

RADIATION DAMAGE IN DIAMOND: Experiments using DFXM with the BFXM and XRD probes gave a detailed lattice-level view of a "radiation resilient" material—diamond. Single-crystal diamond is well-known to graphitize with sufficient X-ray radiation intensity, requiring ~3 eV per atom to begin the amorphization process. Our

experiments (~0.0017 eV/atom) observed localized loss of long-range order from cumulative radiation damage over long timescales using, multiple probes for cross-validation. Initially, we irradiated the diamond at full XFEL flux for ~24 hours during alignment and observed that the single-crystal's diffraction intensity had diminished by 7 orders of magnitude over this time. We subsequently imaged this transformation in a fresh region of the sample with both DFXM and BFXM, and observed streaks that appeared only in the DFXM images over 30 minutes. As this experiment at the PAL-XFEL used a 31-CRL stack for 9.7 keV photons, our imaging sensitivity showed us dark features in our images where the local strain was $\varepsilon \sim 10^{-3}$. The streaks that appeared gradually over the 46,000 XFEL shots originated from local changes in the structure, either from graphitization or localized strain. Triggering difficulties with the pco.edge detectors that we required prevented us from collecting >2 counts per pixel, preventing our results from providing the unambiguous results that are required for this high-impact publication. Further experiments with the higher quantum-efficiency detectors will enable us to collect the results required for the manuscript to be completed. The findings from these results are essential to understand the mechanism and threshold of radiation damage in the most radiation resilient material, in order to inform both the timescales of planetary formations and the damage thresholds for X-ray optics. We will complete these measurements during our upcoming experiments in the 2nd half of 2020.

This work was performed in part under the auspices of the U.S. Department of Energy by Lawrence Livermore National Laboratory under Contract DE-AC52-07NA27344.

References:

1. Bulatov, V. V. *et al.* Dislocation multi-junctions and strain hardening. *Nature* **440**, 1174–1178 (2006).
2. Zhao, K., Pharr, M., Vlassak, J. J. & Suo, Z. Fracture of electrodes in lithium-ion batteries caused by fast charging. *J. Appl. Phys.* **108**, 073517 (2010).
3. Zepeda-Ruiz, L. A., Stukowski, A., Oppelstrup, T. & Bulatov, V. V. Probing the limits of metal plasticity with molecular dynamics simulations. *Nature* **550**, 492–495 (2017).
4. Li, J., Van Vliet, K. J., Zhu, T., Yip, S. & Suresh, S. Atomistic mechanisms governing elastic limit and incipient plasticity in crystals. *Nature* **418**, 307–310 (2002).
5. Tuller, H. L. & Bishop, S. R. Point Defects in Oxides: Tailoring Materials Through Defect Engineering. *Annu. Rev. Mater. Res.* **41**, 369–398 (2011).
6. Simons, H. *et al.* Dark-field X-ray microscopy for multiscale structural characterization. *Nat. Commun.* **6**, 6098 (2015).
7. Campbell, G. H., McKeown, J. T. & Santala, M. K. Time resolved electron microscopy for in situ experiments. *Appl. Phys. Rev.* **1**, 041101 (2014).
8. Abbey, B. From grain boundaries to single defects: A review of coherent methods for materials imaging in the X-ray sciences. *J. Miner. Met. Mater. Soc.* **65**, 1183–1201 (2013).
9. Gorkhover, T. *et al.* Femtosecond and nanometre visualization of structural dynamics in superheated nanoparticles. *Nat. Photonics* **10**, 93–97 (2016).
10. Chapman, H. N. *et al.* Femtosecond diffractive imaging with a soft-X-ray free-electron laser. *Nat. Phys.* **2**, 839–

843 (2006).

11. Sandberg, R. L. *et al.* Ultrafast Imaging of Shocked Material Dynamics with X-ray Free Electron Laser Pulses. in *CLEO: 2014 Postdeadline Paper Digest* STh5C.8 (Optical Society of America, 2014). doi:10.1364/CLEO_SI.2014.STh5C.8
12. Sakdinawat, A. & Attwood, D. Nanoscale X-ray imaging. *Nat. Photonics* **4**, 840–848 (2010).
13. Kim, D. *et al.* Active site localization of methane oxidation on Pt nanocrystals. *Nat. Commun.* **9**, 3422 (2018).
14. Clark, J. N. *et al.* Three-dimensional imaging of dislocation propagation during crystal growth and dissolution. *Nat. Mater.* **14**, 780–784 (2015).
15. Meyers, M. A., Mishra, A. & Benson, D. J. Mechanical properties of nanocrystalline materials. *Prog. Mater. Sci.* **51**, 427–556 (2006).
16. Poulsen, H. F. *et al.* X-ray diffraction microscopy based on refractive optics. *J. Appl. Crystallogr.* **50**, 1441–1456 (2017).